



# Machining performance in longitudinal-torsional ultrasonic-assisted core drilling of CFRP

ZiQiang Zhang<sup>1</sup> · Feng Jiao<sup>1</sup> · YuanXiao Li<sup>1</sup> · Ying Niu<sup>1</sup> · JingLin Tong<sup>1</sup>

Received: 16 November 2022 / Accepted: 17 November 2022 / Published online: 30 November 2022  
© The Author(s), under exclusive licence to Springer-Verlag London Ltd., part of Springer Nature 2022

## Abstract

Ultrasonic vibration–assisted core drilling has achieved some beneficial results in carbon fiber–reinforced plastics (CFRP) hole machining. Among them, longitudinal-torsional ultrasonic-assisted core drilling (LTUACD) shows more significant advantages in decreasing cutting force and reducing delamination defects and other aspects compared to longitudinal ultrasonic-assisted core drilling (LUACD). However, the reduction mechanism of cutting force and delamination defects in LTUACD is still not clear enough. Therefore, this paper researched the machining performance of LTUACD of CFRP. Specifically, the cutting force in LTUACD of CFRP is analyzed based on hertz contact theory and indentation depth theory. Then, a series of experiments were conducted to verify the analysis. And delamination suppression mechanism was discussed from the aspects of surface morphology of hole wall, exit morphology of hole, and bottom surface morphology of blind hole. The results show that the cutting force is significantly reduced in LTUACD compared to conventional core drilling (CCD) and LUACD due to the additional torsional vibration of tool, which changes the contact state between abrasive grain and material. Therefore, the exit delamination is further suppressed. In addition, the adhesion phenomenon of chips on the tool is also reduced, which enhances the tool cutting ability to obtain even fiber fracture surfaces and greatly improves hole quality.

**Keywords** CFRP · Exit delamination · Longitudinal-torsional ultrasonic-assisted core drilling · Cutting force · Surface morphology

## 1 Introduction

Carbon fiber–reinforced plastics (CFRP) have been extensively applied in aerospace, defense, and medical service fields by virtue of outstanding mechanical properties, such as high specific strength and superior corrosion resistance [1, 2]. Mechanical drilling is commonly adopted during hole making processes, for fastening structural assembly. Nevertheless, due to anisotropic and heterogeneous of CFRP, delamination and tear defects are prone to appear. These defects, especially delamination, reduce fatigue strength and lead to rejection of CFRP parts in assembling process [3]. In recent years, to restrain delamination, various drills of novel geometries have been developed, for instance step drill, saw drill, and core drill [4]. Tsao et al. [5] found that because thrust force is scattered on periphery, the core drill induced

slighter delamination compared to twist drill by Taguchi analysis. Cadorin et al. [6] pointed out thrust force during conventional core drilling (CCD) is significantly smaller than that in twist drilling, because of eliminated chisel edge effect. However, exclusion of rod chips is difficult in CCD. Chip exclusion block results in severe outlet delamination.

To solve chip exclusion issue and reduce delamination, longitudinal ultrasonic-assisted core drilling (LUACD), which is also called rotary ultrasonic machining (RUM), including grinding and vibration machining, an unconventional machining method, has been applied to hole machining processes. Peel-up delamination, which is typical defect in twist drilling, was not generated for LUACD of CFRP [7]. Feng et al. [8] experimentally investigated the feasibility of LUACD of CFRP from the aspect of influences of process parameters (rotary speed and feed rate) and vibration parameter (ultrasonic amplitude) on thrust force and surface roughness. The results showed that LUACD of CFRP is a high-efficiency and machining quality process. Smooth machining surface was generated via high rotary speed and low feed rate. Zhang et al. [9] conducted finite

✉ Feng Jiao  
jiaofeng@hpu.edu.cn

<sup>1</sup> School of Mechanical and Power Engineering, Henan Polytechnic University, Jiaozuo 454003, Henan, China

element analysis to research delamination development and build association of thrust force and delamination thickness for LUACD of CFRP. Lv et al. [10] carried out research on effects of high-frequency vibration on hole integrity in LUACD of CFRP, which reduced thrust force and surface roughness by inducing smoothing effects, and developed critical conditions of delamination initiation. Ning et al. [11] performed single abrasive scratching experiments to research material removal mechanism of LUACD of CFRP in contrast to CCD, found CFRP is extensively removed by brittle removal mode in conventional test, and scratching process with additional ultrasonic generates ductile removal zone by analyzing geomorphology of scratched groove, cross-sectional contour. Wu et al. [3] investigated influences of process parameters (feed rate and spindle speed), vibration parameter (ultrasonic vibration), and backup ways on internal delamination on hole wall in CFRP drilling, as well as variable feed rate machining strategy. Baraheni et al. [12] studied influences of process parameters (cutting speed and feed rate), material parameter (thickness), and ultrasonic vibration on thrust force and delamination. Then, regression models were established to predict delamination, and results showed that the influence of thickness on delamination is greatest by statistical evaluation. Thirumalai et al. [13] performed experimental study on LUACD of CFRP in cryogenic environment. The microscopic images of tool wear, burr formation, and hole surface morphology were analyzed and examined. Shi et al. [14] carried out research on evaluation of surface roughness of LUACD of CFRP by adapting a novel evaluation method based on sampling array. Li et al. [15] reported chip removal research on LUACD of CFRP. The chip removal principle on LUACD of CFRP was presented, and the experiment was carried out. The results indicated that chip blockage phenomenon was significantly improved when vibration amplitude exceeded  $5\ \mu\text{m}$  compared with CCD. The sticking chip, blocking rod, thrust force, tool wear, and cutting temperature were obviously reduced. Amini et al. [16] experimentally investigated thrust force and dimensional tolerances including roundness and cylindricity in LUACD of CFRP. The results showed that thrust force, roundness, and cylindricity reduced by up to 30%, 80%, and 72%, respectively, compared to conventional

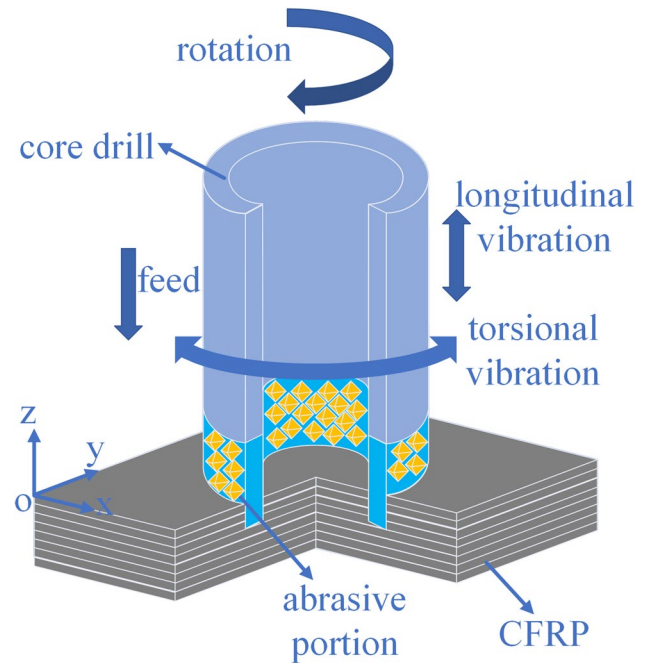
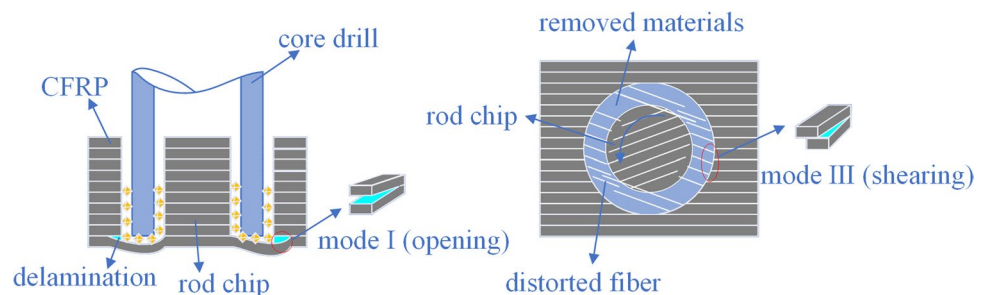


Fig. 1 LTUACD of CFRP

drilling. Afterwards, vibration is more influential than other machining parameters on improvement of hole accuracy. The above researches were related to one-dimensional LUACD developed on ultrasonic-assisted machining. Though processing performance has been enhanced via this process, its machining capacity was restricted by extreme conditions [17].

With the development of ultrasonic-assisted machining technology, two-dimensional vibration has been applied to ultrasonic-assisted core drilling by virtue of its excellent performance. Wang et al. [18] conducted experimental study on longitudinal-torsional ultrasonic-assisted core drilling (LTUACD) of quartz glass. The results demonstrated that cutting force was reduced by 55%, hole outlet edge chipping size was reduced by 45% averagely, and the quality of hole wall was improved compared to LUACD. Compared to conventional drilling, Geng et al. [19] presented an investigation on tool wear mechanism of rotary ultrasonic elliptical

Fig. 2 Exit delamination of CCD of CFRP



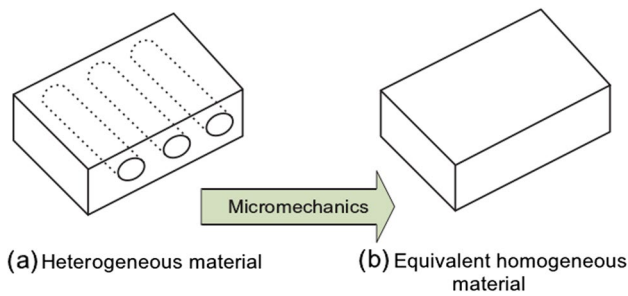


Fig. 3 CFRP micromechanics analysis [22]

machining (RUEM) of CFRP. The trial results indicated that tool life increased by 28% in RUEM than that in conventional drilling, and chip blockage phenomenon was significantly improved. Chen et al. [17] performed LTUACD of ZrO<sub>2</sub> ceramics research. Experimental results showed that cutting force and grain wear were significantly reduced, and hole surface quality was improved compared to conventional machining. Geng et al. [1] observed and analyzed delamination generation during CCD and RUEM of CFRP. The experimental results showed that, compared with CCD, hole exit delamination was reduced by 5.4~19.3% at 1/2 plies and 0.7~8.4% at 2/3 plies under feed rate of 0.05~0.1 mm/r. After that, delamination restrain mechanism of RUEM was discussed. Liu et al. [20] introduced and analyzed cutting force model and chip removal phenomenon in RUEM of CFRP. The experimental results demonstrated that compared to conventional drilling, chip evacuation capacity and tool service life were improved, cutting force was reduced, and delamination at hole exit was prevented. Geng et al. [21] conducted research on cutting temperature in RUEM and CCD. The reasons of temperature decrement and chip sticking restrain of RUEM were discussed. The experimental outcomes demonstrated that in contrast to CCD, RUEM decreased temperature by 18.8% and 13.1% with feed rate of 0.075 and 0.15 mm/r, respectively. In addition, better microstructure was obtained in RUEM.

Though research on LTUACD of brittle materials has been conducted in recent years, there are few researches on machining performance in LTUACD of CFRP. In particular,

the research on reduction mechanism of cutting force and delamination defects in LTUACD of CFRP has not been found. Therefore, this paper analyzed the cutting force in LTUACD of CFRP in theory. Then, a series of trails were conducted to verify the analysis. Moreover, influences of fiber orientation on delamination generation were mentioned. Finally, delamination suppression mechanism was revealed from the aspects of surface morphology of hole wall, exit morphology of hole, and bottom surface morphology of blind hole.

## 2 Cutting force analysis in LTUACD of CFRP

The schematic diagram of LTUACD of CFRP is shown in Fig. 1. The delamination of CFRP in CCD is illustrated in Fig. 2; as twist drilling of CFRP, the cutting force is a significant factor which affects initiation of delamination. Therefore, it is meaningful for suppressing delamination defects of CFRP to reduce cutting force of tools.

Micromechanics analysis is used to represent the heterogeneous CFRP workpiece as an equivalent homogeneous material [22], as shown in Fig. 3. The action of grain on workpiece is same as Vickers indenter in CCD of CFRP, as shown in Fig. 4 (a). Combining Hertz contact theory, the indentation depth is relatively small when abrasive starts to contact the surface of the workpiece. Then, the material is scratched and deformed, and the plastic deformation region generates. The region would enlarge with movement of abrasive grain and increase of indentation depth. The radial crack generates when indentation depth is maximum. Furthermore, due to internal tensile stress of material, the lateral crack generates and propagates to the surface of the workpiece, and the material is removed in brittle fracture mode. The cracks initiate and propagate with movement of abrasive grain, which leads to the formation of chip at macro scale.

According to Cong’s research result [22], the cutting force  $F_1$  of rotary ultrasonic machining (which is also called longitudinal ultrasonic-assisted core drilling) of CFRP can be obtained from the following equation:

Fig. 4 Interaction of abrasive grain and material: (a) CCD, (b) LUACD and LTUACD

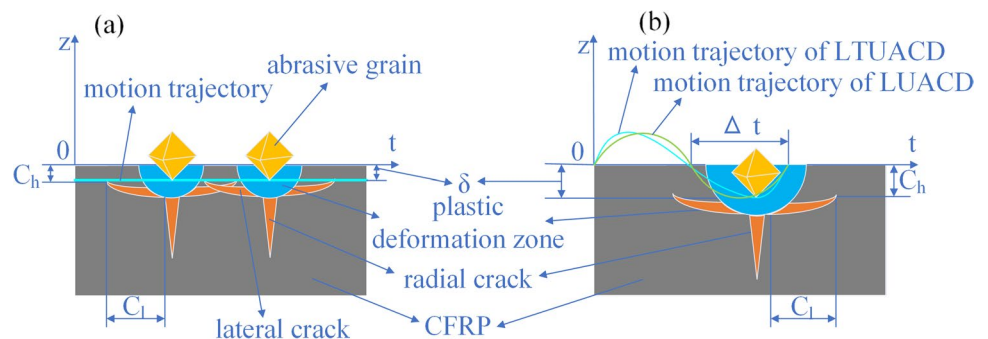
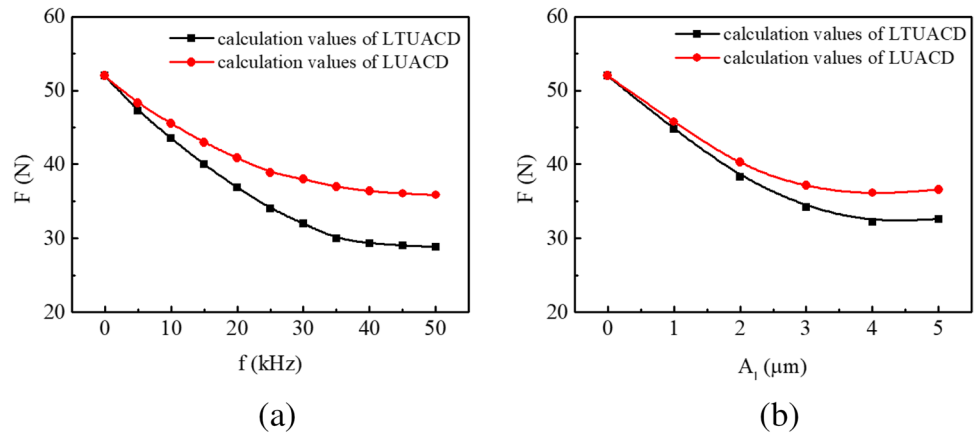


**Fig. 5** Cutting force with regard to **a** frequency at  $n = 3500r/min$ ,  $v_f = 10\text{mm/min}$ ,  $A_f = 3\mu\text{m}$  et al. **b** Longitudinal ultrasonic amplitude at  $n = 3500r/min$ ,  $v_f=10\text{ mm/min}$ ,  $f = 35\text{kHz}$  et al. in LTUACD and LUACD of CFRP



$$\left\{ \begin{aligned} v_f \frac{\pi(D_o^2 - D_i^2)}{4} &= \frac{KN^{\frac{1}{4}} \pi^2 n(D_o + D_i)}{180} \left( \frac{F_L}{K_{IC}} \right)^{\frac{3}{4}} (\delta d - \delta^2)^{\frac{1}{2}} \left[ \frac{1}{2} - \frac{1}{\pi} \arcsin\left(1 - \frac{\delta}{A_f}\right) \right]^{\frac{1}{4}} \\ F_L &= \frac{8^{\frac{1}{2}} NE d^{\frac{1}{2}} \delta^{\frac{3}{2}}}{3(1-\nu^2)} \left[ \frac{1}{2} - \frac{1}{\pi} \arcsin\left(1 - \frac{\delta}{A_f}\right) \right] \end{aligned} \right. \quad (1)$$

In this paper, the accomplished longitudinal-torsional ultrasonic vibration is synchronous vibration. When the tool is exerted longitudinal-torsional ultrasonic vibration, the contact time of abrasive grain and workpiece during a vibration cycle is demonstrated in Fig. 4 (b).

$$\Delta t = \lambda \left[ \frac{3}{2f} - \frac{1}{\pi f} \arcsin\left(\frac{\delta}{A_f}\right) \right] \quad (2)$$

where  $\lambda$  marks unloading effect of torsional vibration when abrasive grain is pulled out from material [18].

Owing to additional ultrasonic vibration of tool, the contact of abrasive grain and workpiece becomes separated intermittent impulse contact. The effective cutting length of abrasive grain exerted longitudinal-torsional ultrasonic vibration in a vibration cycle:

**Table 1** Properties of CFRP

Properties	Unit	Value
Density	$\text{g/cm}^3$	1.6
Longitudinal elasticity modulus	GPa	132
Transverse elasticity modulus	GPa	11
Carbon fiber volume fraction	%	67
Carbon fiber	–	T700
Epoxy	–	69A
Dimension	mm	240×120×5
Poisson ratio	–	0.29
Shear modulus	GPa	5.2
Tensile strength	MPa	2179
Compression strength	MPa	168

$$l = \frac{\Delta t}{T} \int_0^T \sqrt{v_x^2 + v_y^2 + v_z^2} dt \quad (3)$$

where abrasive grain motion speed  $v_x = -\frac{D_o + D_i}{4} \sin\left[\frac{4A_f \sin(2\pi ft)}{D_o + D_i} + \frac{\pi n}{30} t\right]$ ,  $v_y = \frac{D_o + D_i}{4} \cos\left[\frac{4A_f \sin(2\pi ft)}{D_o + D_i} + \frac{\pi n}{30} t\right]$ ,  $v_z = -\frac{v_f}{60} + 2A_f f \pi \cos(2\pi ft)$ .

The applied fracture toughness of CFRP is dynamic fracture toughness  $K_{ID}$ , based on literature [23],  $K_{ID} = 0.3K_{IC}$  and the number of abrasive grains participating in the machining process  $N_1 = \varepsilon \sigma d_1 N$  according to literature [24].

Apply Cong’s calculation approach, and by simplifying the calculation, the cutting force of longitudinal-torsional ultrasonic-assisted core drilling of CFRP is

$$F = \left( \frac{3\pi v_f}{f \int_0^T \sqrt{v_x^2 + v_y^2 + v_z^2} dt} \right)^{\frac{10}{11}} \frac{(1-\nu^2)^{\frac{5}{22}} H_v^{\frac{50}{43}} K_{ID}^{\frac{5}{11}} \tan^{\frac{7}{11}} \frac{\beta}{2}}{0.226^{\frac{20}{11}} E^{\frac{35}{44}} A_f^{\frac{1}{22}} \frac{131}{66}} \left( 0.051 \sin \frac{\beta}{2} \right)^{\frac{1}{44}} (\varepsilon \sigma d_1 \lambda)^{\frac{1}{11}} (D_o^2 - D_i^2) \left( \frac{2.64 \times 10^{-5} C}{d^3 \rho} \right)^{\frac{2}{33}} \quad (4)$$

where  $v_f$ ,  $f$ ,  $T$ ,  $D_o$ ,  $D_i$ ,  $A_f$ ,  $n$ , and  $A_1$  are feed speed, vibration frequency, vibration cycle, outside diameter, inside diameter, torsional amplitude, rotation speed, and longitudinal amplitude of tool, respectively;  $E$ ,  $H_v$ , and  $\nu$  are elastic modulus, Vickers hardness, and Poisson ratio of CFRP, respectively;  $\beta$ ,  $d_1$ ,  $C$ ,  $\rho$ , and  $d$  are apical angle, diagonal length, concentration, density, and edge length of abrasive grain;  $\lambda$  is

**Table 2** Parameters of core drill

Parameters	Unit	Value
Outer diameter	mm	8
Inner diameter	mm	7
Mesh size	no	60–70
Abrasive grain concentration	%	100
Abrasive grain size	$\mu\text{m}$	0.25
length	mm	50



coefficient that denotes influence of torsional vibration on machining process with  $0.5 < \lambda < 1$ ;  $\epsilon$  is ratio of uncovered abrasive grains;  $\sigma$  is ratio of max exposed height to diameter of abrasive grain.

Figure 5 presents influence of frequency and amplitude on cutting force for LTUACD and LUACD of CFRP under following conditions:  $v_f = 10\text{mm/min}$ ,  $f = 35\text{kHz}$ ,  $D_o = 8\text{mm}$ ,  $D_i = 7\text{mm}$ ,  $A_t = 1.5\mu\text{m}$ ,  $n = 3500\text{r/min}$ ,  $A_l = 3\mu\text{m}$ ,  $v_{cf} = 0.3$ ,  $v_m = 0.4$ ,  $V_f = 67\%$ ,  $V_m = 33\%$ ,  $E_f = 230\text{GPa}$ ,  $E_m = 4.5\text{GPa}$ ,  $H_v = 0.6\text{GPa}$ ,  $G_f = 2\text{J/m}^2$ ,  $G_m = 500\text{J/m}^2$ ,  $\beta = 90^\circ$ ,  $\epsilon = 26\%$ ,  $\sigma = 0.33$ ,  $d_1 = 0.25\mu\text{m}$ ,  $\lambda = 0.8$ ,  $C = 100\%$ ,  $d = 0.17\mu\text{m}$ ,  $\rho = 3.52 \times 10^{-3}\text{g/mm}^3$ . From above, it can be seen that cutting force of tool is significantly reduced within a certain range in LTUACD of CFRP. Besides, compared to LUACD, the cutting force of tool in LTUACD of CFRP is

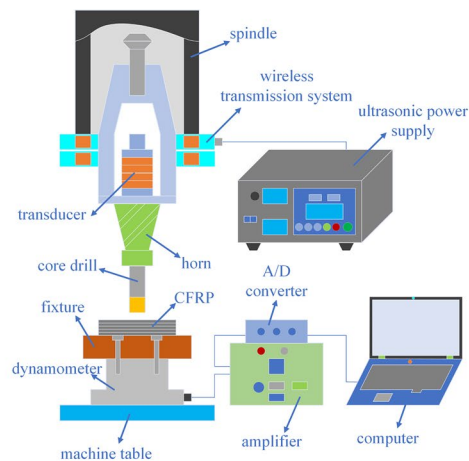
further reduced. Therefore, the process can reduce generation of delamination defects.

### 3 Experimental conditions and methods

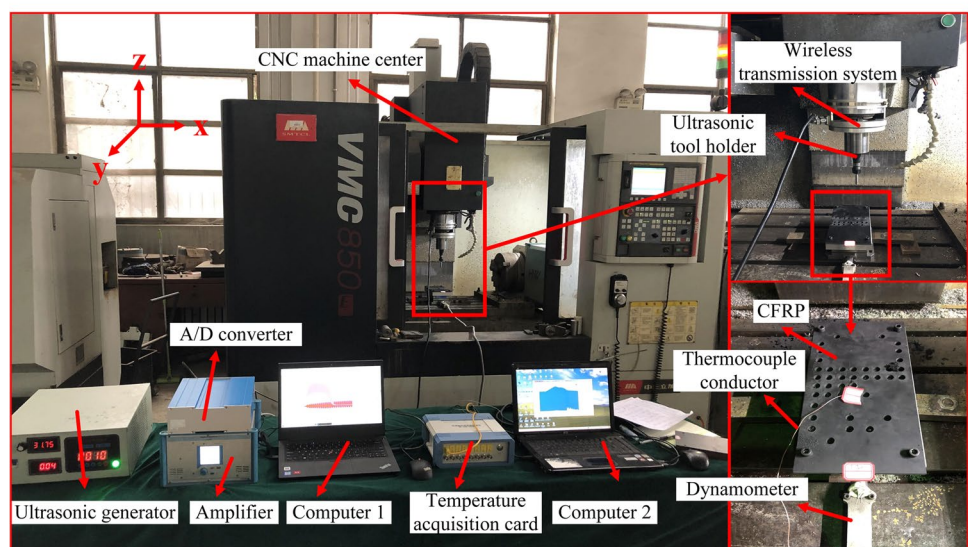
#### 3.1 tool and workpiece

The workpiece used in trials is unidirectional CFRP laminated, material properties are listed in Table 1, and some of them were calculated by micromechanical analysis. The employed tool is electroplated diamond core drill (Zhengzhou Research Institute for Abrasive and Grinding, China) with detailed specifications listed in Table 2.

**Fig. 6** Experimental set-up: **a** schematic diagram and **b** trial site



(a)



(b)

### 3.2 Experimental apparatus and set-up

The experiments were performed on a CNC machine center (VMC-850E, Shenyang Machine Tool Works, China), equipped with ultrasonic vibration devices. The configuration of experimental set-up is schematically illustrated in Fig. 6. The longitudinal-torsional coupled vibration was fulfilled by adding helical flutes on horn, and amplitude ratio of torsional to longitudinal is 0.52.

The contrast experiments of CCD, LUACD, and LTUACD were performed to evaluate processing performance. Owing to restriction of experimental set-up, ultrasonic power was fixed, while spindle speed, feed rate, and ultrasonic amplitude varied. Every experiment was repeated three times, and average value was used as final result. The specifications of experimental conditions are presented in Table 3, and amplitude in table is longitudinal amplitude, emphasizing that two CFRP laminates were machining at the same time and the underlying CFRP plate was playing a role in supporting. Besides, the trails were conducted without any coolant. Moderate spindle rotational speed and low feed rate were selected for experiments [20].

### 3.3 Measurement procedures

In the machining process, a three-way piezoelectric ceramic dynamometer (KISTLER-9257B) was used to measure cutting force. Original cutting force contained direct current (mean cutting force) and ultrasonic frequency sinusoid alternating current components. Because nature frequency of dynamometer is much lower than ultrasonic vibration frequency, it is unable to sample high-frequency sinusoid alternating current constituent of original cutting force. In contrast, cutting force mean value is unrelated to above-mentioned. Therefore, cutting force mean value was used to evaluate processing performance. The surface morphology of hole wall was observed by scanning electron microscope (SEM). The hole exit delamination and the bottom surface morphology of blind hole of CFRP were viewed by super depth of field microscope. Specifically, two-dimensional delamination factor  $F_a$  is employed to assess exit [25], as shown in Fig. 7:

$$F_a = \frac{A_d - A_n}{A_n} \quad (5)$$

where  $A_d$  is area of concentric circle of hole including delamination defects;  $A_n$  is nominal area of hole.

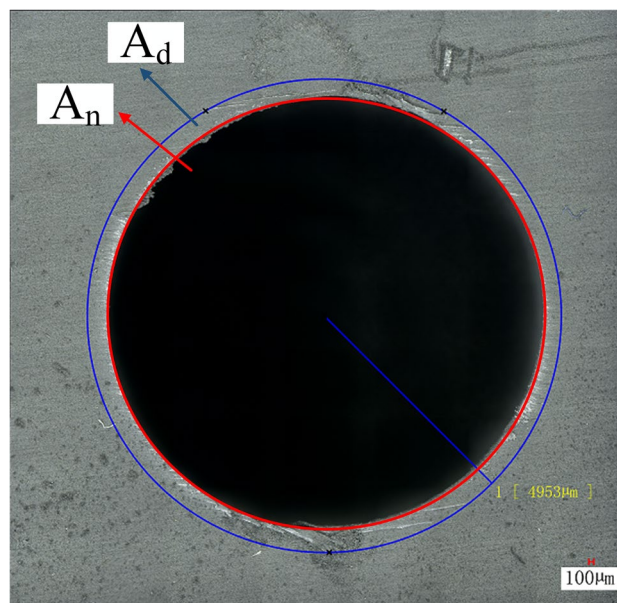
**Table 3** Experimental conditions

Variables	Unit	Value
Spindle speed	r/min	2000, 2500, 3000, 3500
Feed rate	mm/min	10, 13, 16, 19
Ultrasonic amplitude	$\mu\text{m}$	0, 1, 2, 3

## 4 Results and discussion

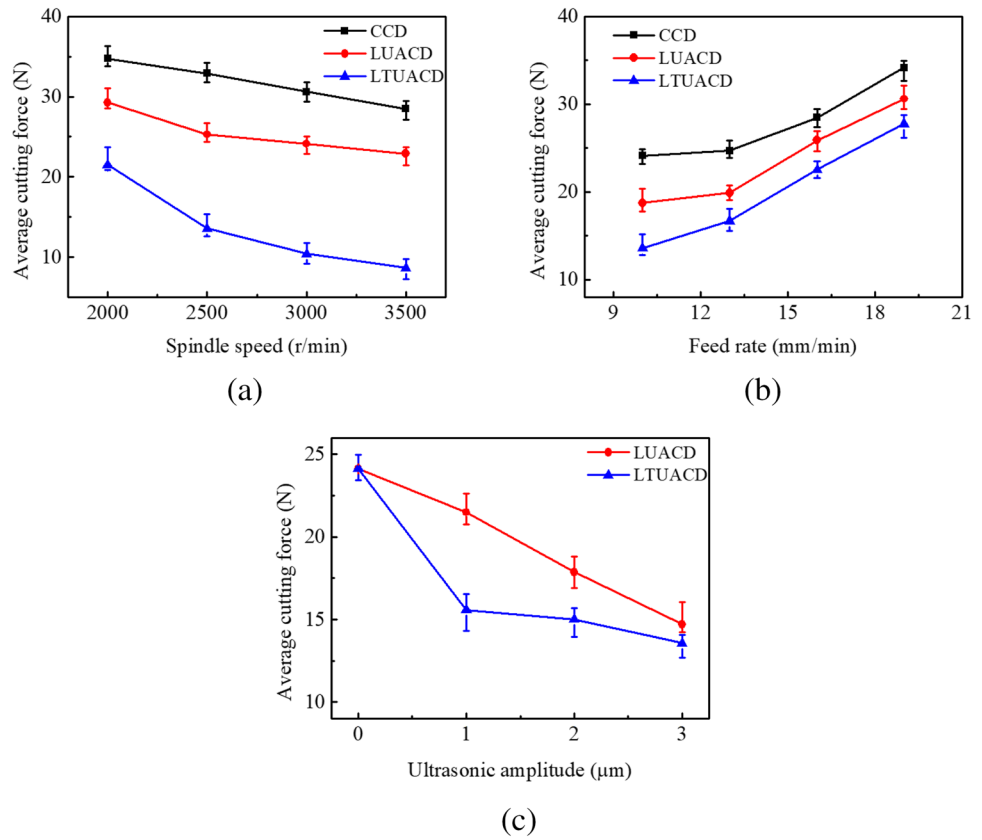
### 4.1 Cutting force

Figure 8 presents the influence of processing parameters on cutting force in CCD, LUACD, and LTUACD of CFRP. The cutting force reduction ratio is used to evaluate the processing performance. It is observed that in Fig. 8a, compared to CCD, cutting force is reduced by 15.7~23.1% in LUACD and 38.1~69.7% in LTUACD. Compared with LUACD, cutting force is reduced by 26.6~62.3% in LTUACD. In Fig. 8b, compared to CCD, cutting force is reduced by 9.1~22.3% in LUACD and 18.8~43.8% in LTUACD. Compared with LUACD, cutting force is reduced by 9.3~27.6% in LTUACD. In Fig. 8c, compared with LUACD, cutting force is reduced by 7.7~27.5% in LTUACD. The cutting force decrease of LTUACD is because of the intermittent cutting phenomenon. In addition, the attached torsional vibration reduces the contact time of abrasive grain and



**Fig. 7** Evaluation method

**Fig. 8** Cutting force with regard to **a** spindle speed at  $v_f = 10\text{mm/min}$ ,  $A = 1\mu\text{m}$ ; **b** feed rate at  $n = 4000\text{r/min}$ ,  $A = 1\mu\text{m}$ ; **c** ultrasonic amplitude at  $n = 4000\text{r/min}$ ,  $v_f = 10\text{mm/min}$  in CCD, LUACD, and LTUACD



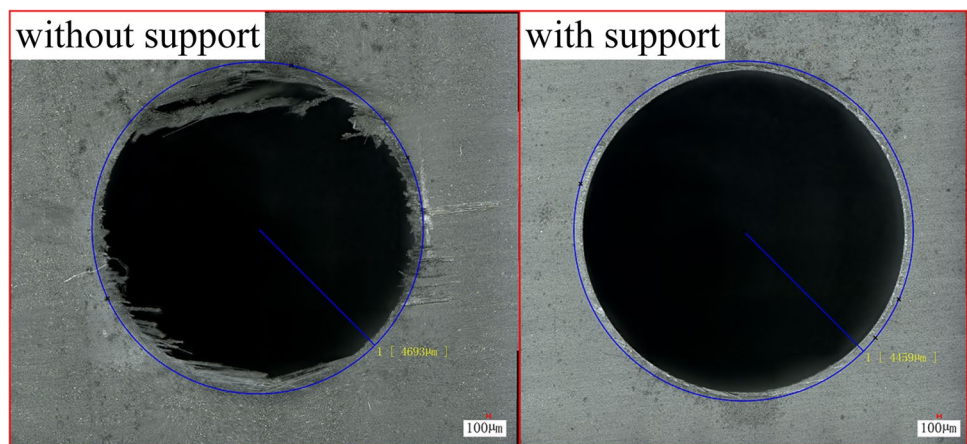
material, which further enhances the intermittent cutting phenomenon. Moreover, the increasing cutting force has harmful influence on keeping validity and stability of ultrasonic machining [26]. The higher the spindle speed and the lower the feed rate, the more contact time of abrasive grain and material, the more obvious the effect of intermittent cutting, which reduces the cutting force. The larger the amplitude, the more obvious the effect of impact is, which will increase cutting force to a certain extent. This weakens the effect of torsional vibration and affects the stability of ultrasonic vibration. Furthermore, the advantage of ultrasonic

vibration is weakened, which results in the increase of cutting force. Based on the delamination generation mechanism, exit delamination shows direct relationship with cutting force. Therefore, this proves that the cutting force decrease of LTUACD could reduce exit delamination.

### 4.2 Exit delamination

On the one hand, the generation of hole outlet delamination is because of the push out effect of thrust force. On the other hand, it is because of the tear shearing effect of rod

**Fig. 9** CFRP exit morphology of with/without support in CCD





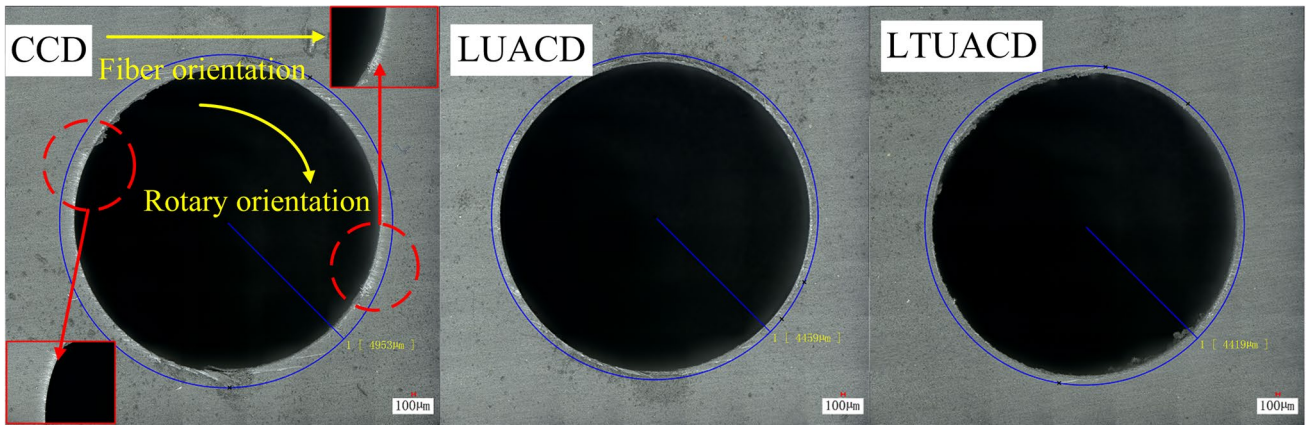
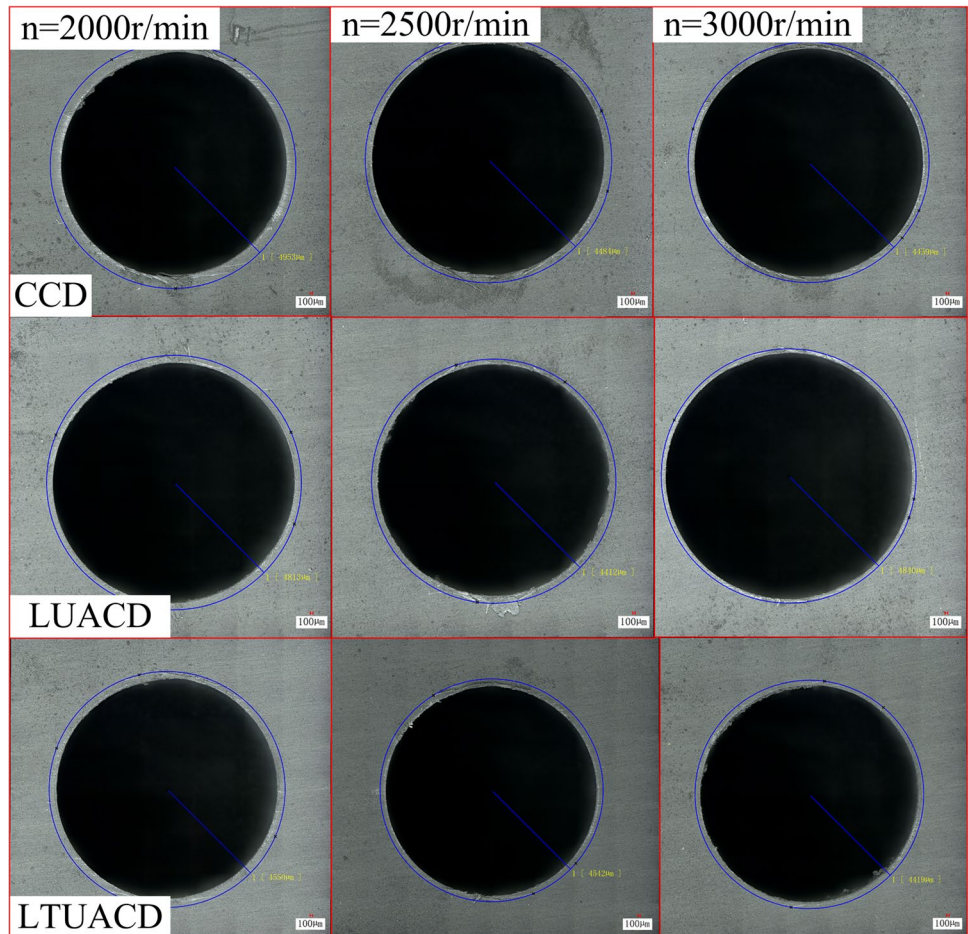


Fig. 10 CFRP exit morphology in CCD, LUACD and LTUACD

chip. Because of the poor back-up, when the tool is penetrating CFRP panel, the at-the-end uncut layer is pushed. And when the remained fibers are cut off, the rod chip, which is located in the interior of the core drill, begins to revolve; therefore, fiber tear and delamination appeared. The generation of outlet delamination is primarily induced by two

types of cracks. One is mode I (opening) cracks, which is triggered by vertical stress. The other is mode III (tearing shear) cracks, which is triggered by out-plane shear stress, as shown in Fig. 2. With the reduction of panel thickness, when the tool penetrates the workpiece, the uncut layers are more easily deformed. Ultimately, the push out delamination,

Fig. 11 CFRP exit morphology with spindle speed at  $v_f = 10\text{mm/min}$ ,  $A = 1\mu\text{m}$  in CCD, LUACD, and LTUACD





which is triggered by mode I cracks, generates when stress is larger than the bonding strength of the material. The shear delamination is appeared because of mode III cracks when rod chip tears the remaining fibers. It needs to be mentioned that mode III cracks are more common compared to mode I cracks when the hole finishes machining.

The hole outlet morphologies of CFRP holes in different processing methods are presented in Fig. 10. Due to the use of backup support, the hole exit delamination is significantly reduced, as shown in Fig. 9. Due to the anisotropy of CFRP, the delamination represented obvious directional characteristics. From Fig. 10, it is found that the delamination around  $135^\circ$  fiber orientation angle is more severe. When fiber cutting angle is blunt angle, fibers suffer bend load because of protrusion of abrasive grain. When thrust force exceeds fiber resin bond strength, tearing action extracts carbon fibers from resin, and the fiber separates from the matrix. Lacking the restriction of resin, the fiber is hard to cut off and is pushed during subsequent machining, leading to delamination. When the fiber orientation angle is acute angle, the fibers suffer shear load owing to shear of abrasive, which can be cut off easily. Therefore, the generated delamination

is relatively small. Besides, compared to CCD and LUACD, the exit delamination of LTUACD is further improved. This is attributed to additional torsional vibration of tool, and the chips separate from the tool and conduce to lesser chip adhesion of tool and tool workpiece friction.

CFRP hole exit morphology at different processing parameters of three processing ways is displayed in Figs. 11, 12, and 13. Figure 14 shows the delamination factor of hole exit delamination regarding processing parameters in CCD, LUACD, and LTUACD of CFRP. Delamination factor reduction ratio is employed to assess processing performance. It is observed that in Fig. 14a, compared to CCD, delamination factor is reduced by 39.1~50% in LUACD and 47.8~67.6% in LTUACD. Compared with LUACD, delamination factor is reduced by 10.3~42.9% in LTUACD. In Fig. 14b, compared to CCD, delamination factor is reduced by 5.6~15.2% in LUACD and 16.7~36.9% in LTUACD. Compared with LUACD, delamination factor is reduced by 8.7~25.6% in LTUACD. In Fig. 14c, compared with LUACD, delamination factor is reduced by 8.7~20% in LTUACD. From Fig. 14, it could be seen that the influence on delamination factor of feed rate is more significant than spindle speed,

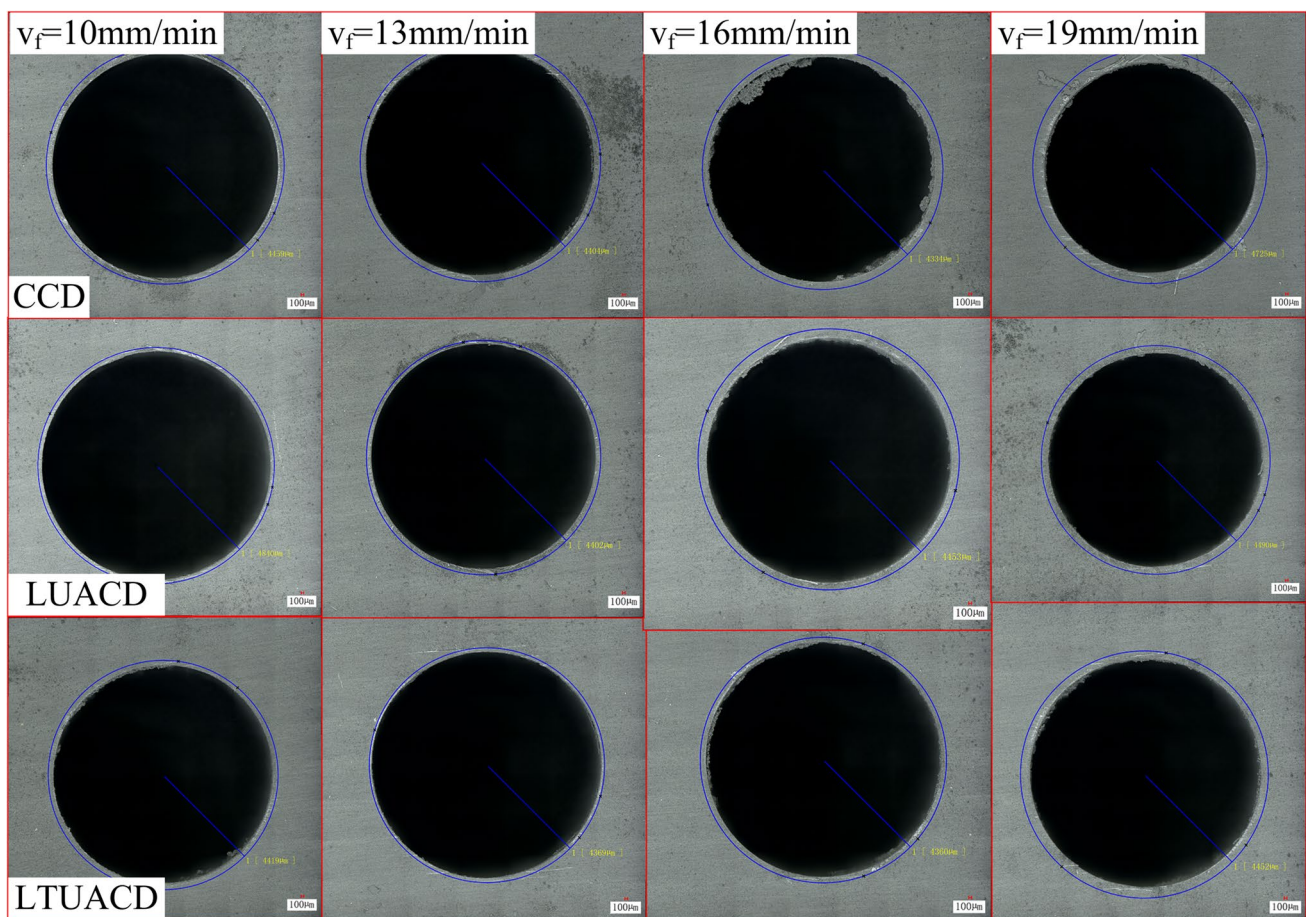


Fig. 12 CFRP exit morphology with feed rate at  $n = 3000$ r/min,  $A = 1\mu\text{m}$  in CCD, LUACD, and LTUACD

which is consistent with finds of twist drilling [27, 28]. The delamination reduction in LTUACD can be attributed to the ultrasonic self-cleaning function. Due to the additional torsional vibration of tool, chips are easier to separate from tool and conduce to lesser tool chip adhesion, which keeps the sharpness of tool. This is beneficial to fiber fracture and reduces tearing shear effect of rod chip. Besides, the effects of ultrasonic vibration on interactive extrusion load of tool end face and machined surface conduced to visible decrement of cutting force, hence reducing exit delamination. According to the above, it can be concluded that the LTUACD process could obtain higher machining efficiency relative to CCD and LUACD.

### 4.3 Bottom surface morphology of blind hole

Figure 15 presents the bottom surface morphology of blind holes in CCD, LUACD, and LTUACD. From the graph, it can be seen that the fractured fibers in the CCD are

needle-shaped, while in LUACD, the volume of fractured fibers is reduced because of influence of high-frequency vibration. Furthermore, in LTUACD, fractured fibers present rice-shaped, whose volume becomes smaller. This is attributed to the additional torsional vibration of tool. From above, it can be concluded that the differences of bottom surface morphology are relevant to the material removal mechanism of three processing methods. In CCD, because the material is in contact with the tool all the time, the tool removed the material via extrusion action of grain. For LUACD, due to the intermittent cutting characteristic, the material is mainly removed by the effect of impact of ultrasonic vibration. This accelerates fiber fracture and reduces the volume of fractured fibers. In LTUACD, owing to the additional torsional vibration of the tool, in circumferential direction, the contact of abrasive grain and material becomes intermittent contact. Except for the shear action of abrasive grain to material, the effect of impact of vibration further accelerates fiber fracture and reduces the volume of fractured fibers, which is helpful for improving material removal efficiency.

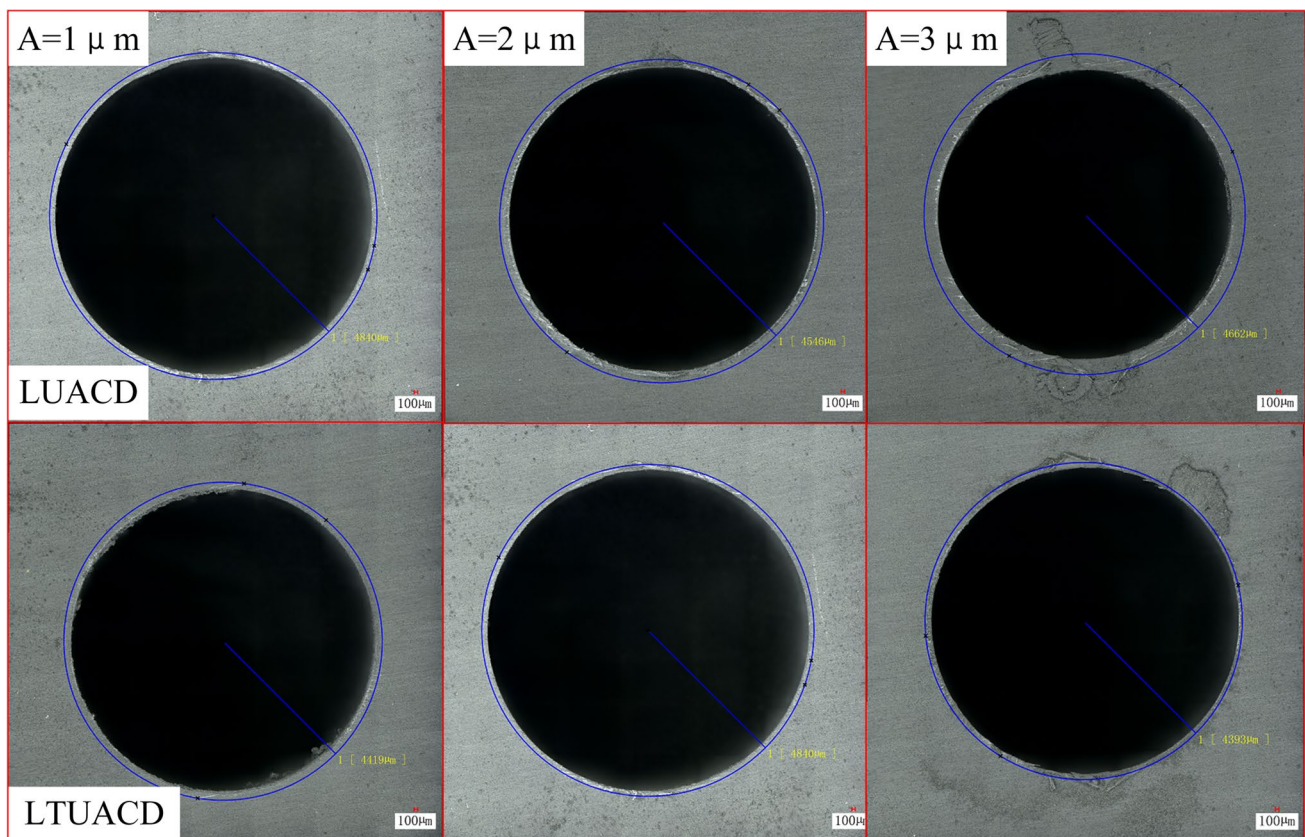
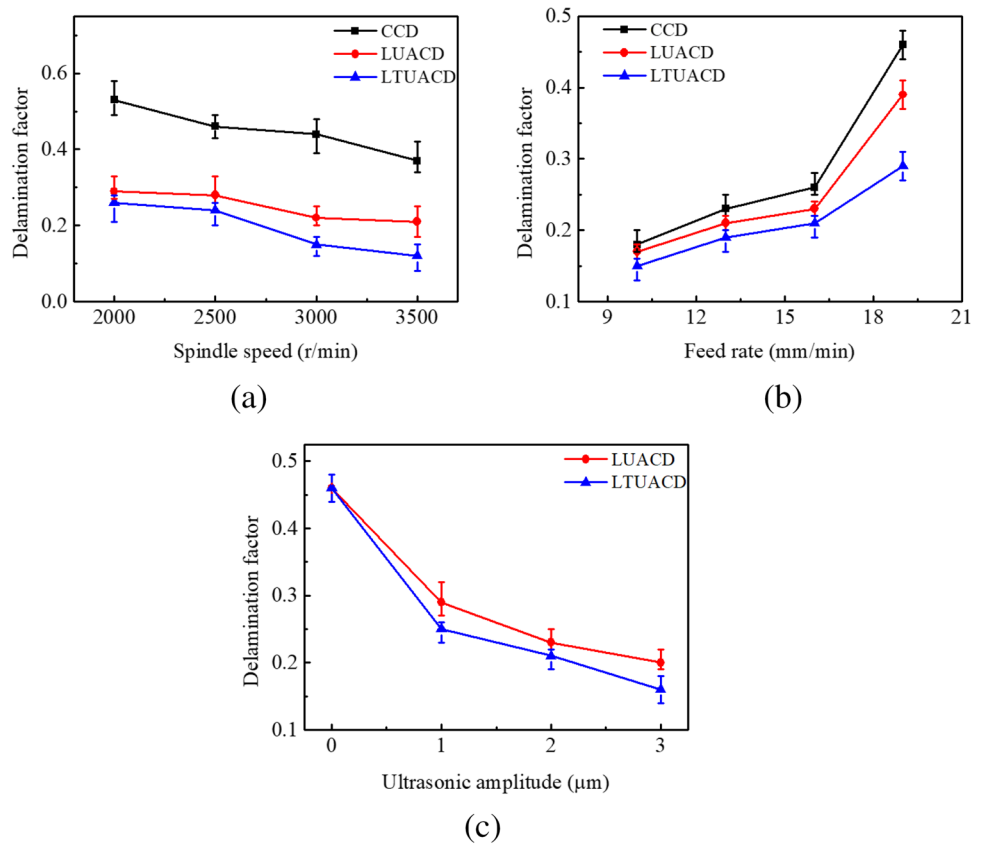


**Fig. 13** CFRP exit morphology with ultrasonic amplitude at  $n = 3000\text{r/min}$ ,  $v_f = 10\text{mm/min}$  in LUACD, and LTUACD



**Fig. 14** Delamination factor with regard to **a** spindle speed at  $v_f = 10\text{mm/min}$ ,  $A = 1\mu\text{m}$ ; **b** feed rate at  $n = 4000\text{r/min}$ ,  $A = 1\mu\text{m}$ ; **c** ultrasonic amplitude at  $n = 2500\text{r/min}$ ,  $v_f = 10\text{mm/min}$  in CCD, LUACD, and LTUACD

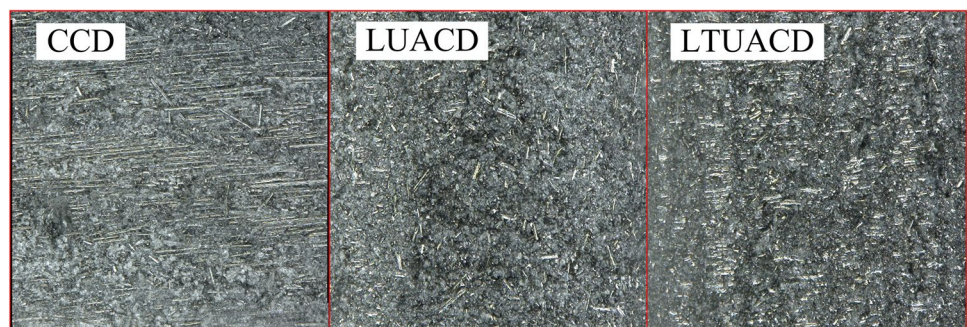


### 4.4 Surface morphology of hole wall

To further verify the above analysis, the microstructures of machined hole surface at different fiber cutting angles in CCD, LUACD, and LTUACD were observed with SEM, as shown in Figs. 16 and 17. The fiber cutting angle  $\theta$ , which is the angle of cutting direction and fiber orientation in clockwise direction, is considered a vital item influencing machining quality of workpiece. Therefore, the microscopic morphologies of four angles of material ( $\theta = 0^\circ, 45^\circ, 90^\circ, 135^\circ$ ) are chosen to contrast. It can be found that in CCD,

the surface of hole wall is relatively rough. In contrast, the surface integrity is obviously improved in LTUACD, and the surface is smooth, and no obvious machining defects. At  $\theta = 0^\circ$  location, the interface de-adhesion of the fibers and resins caused massive fiber pullouts, cracks in the fibers, and fiber expositions in CCD. In LTUACD, the numbers of fiber pullouts and cracks in fibers are significantly reduced. At  $\theta = 45^\circ$  location in CCD, noticeable microchips generated because of fibers fracture were discovered. In the deteriorated resins, noticeable fractured fibers were discovered. In LTUACD, the chipping dimensions are much

**Fig. 15** Bottom surface morphology of blind holes



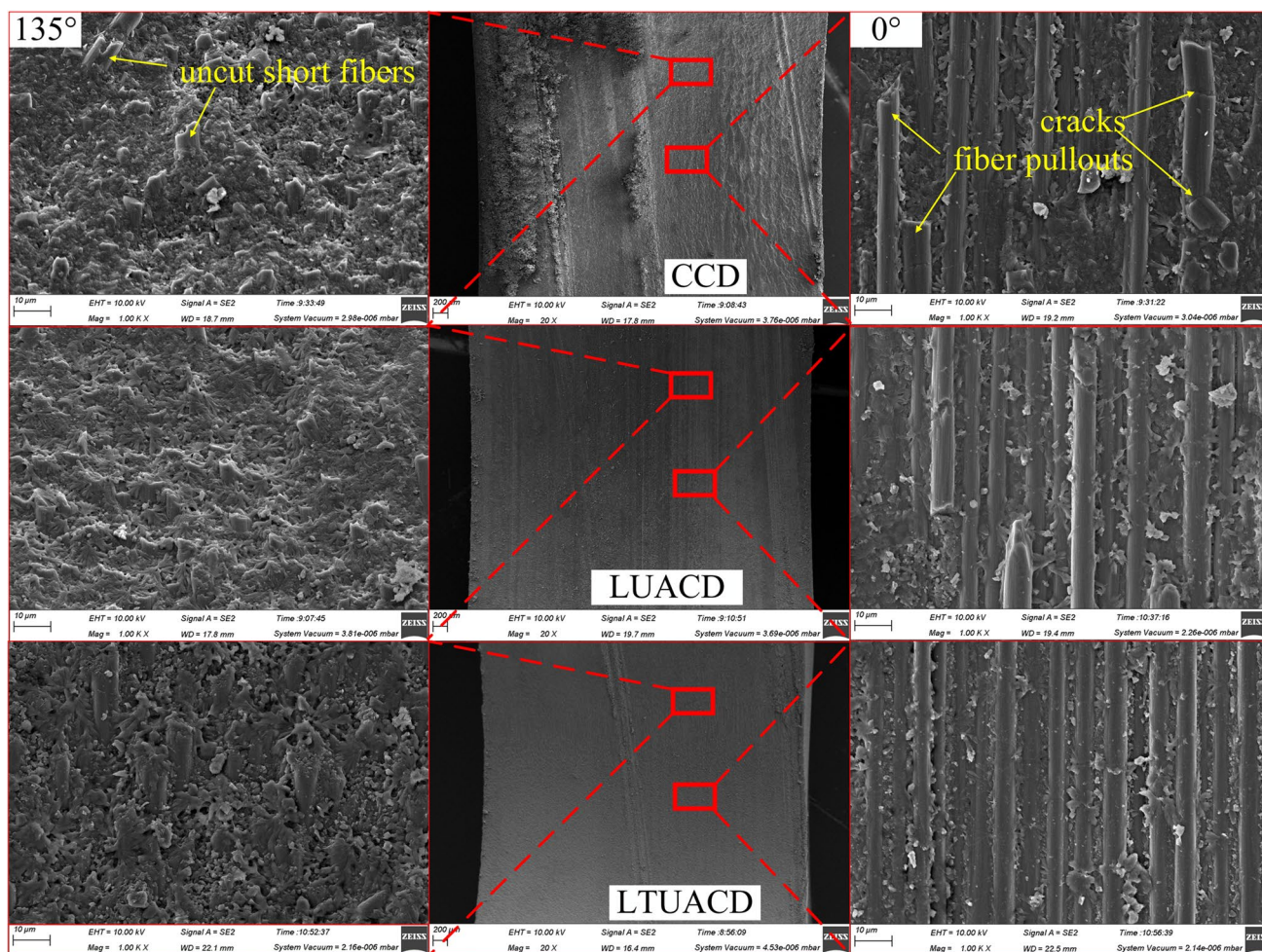


**Fig. 16** Surface morphologies of hole wall at fiber cutting angle of  $0^\circ$  and  $135^\circ$  in CCD, LUACD, and LTUACD ( $n=3000$  r/min,  $v_f=10$  mm/min,  $A=1$   $\mu$ m)

smaller, and the numbers of broken fibers are reduced. At  $\theta=90^\circ$  location in CCD, detectable surface damage (resins degradation) occurred due to thermal effects, which results in the smearing of resins on fibers. Voids or grooves were found due to fiber/matrix pullouts. In LTUACD, the phenomenon of matrix degradation and the numbers of voids are significantly reduced. The fracture surfaces of fibers are flat. Besides, lots of remained uncut fiber chips were discovered with  $\theta=135^\circ$  location in CCD; the phenomenon demonstrated fibers suffered serious bending prior to rupture. The concavo-convex fracture surfaces of fibers occurred. In LTUACD, the fracture surfaces of fibers are relatively flat, which indicates that the mechanism of fiber fracture becomes shear fracture due to the superimposition of ultrasonic vibration, especially the additional torsional vibration.

According to the aforementioned results and figures, it is obvious that shear fracture is a major fracture mode of fiber for LTUACD; however, the bending fracture is a major fracture mode of fiber for CCD. The findings of CCD are

ascribed to terrible chip evacuation situation, awful tool cutting ability, high cutting heat, and serious chip sticking of tool. Because of constant contact of tool and material, the inferior heat conduction is occurred. This leads to that abrasives are covered by sticking chip with ease. This will seriously influence tool cutting capability and then thrust force increases. Furthermore, this results in a great number of chips engaged in the machining process of CFRP, which increases friction of tool and material, so as to give rise to unstable machining process and increase cutting heat. Hence, the fibers are quite difficult to be cut off because of increasing cutting heat. Then, terrible machining surfaces generate. And the matrix damages are also easily occurred. The findings in LTUACD are because the machining process becomes separated cutting state because of additional ultrasonic; chips are difficult to stick on tool because of high-frequency vibration, and machining surface becomes smoother because of reciprocating scratches of abrasives. The ultrasonic self-cleaning function reduces the chip



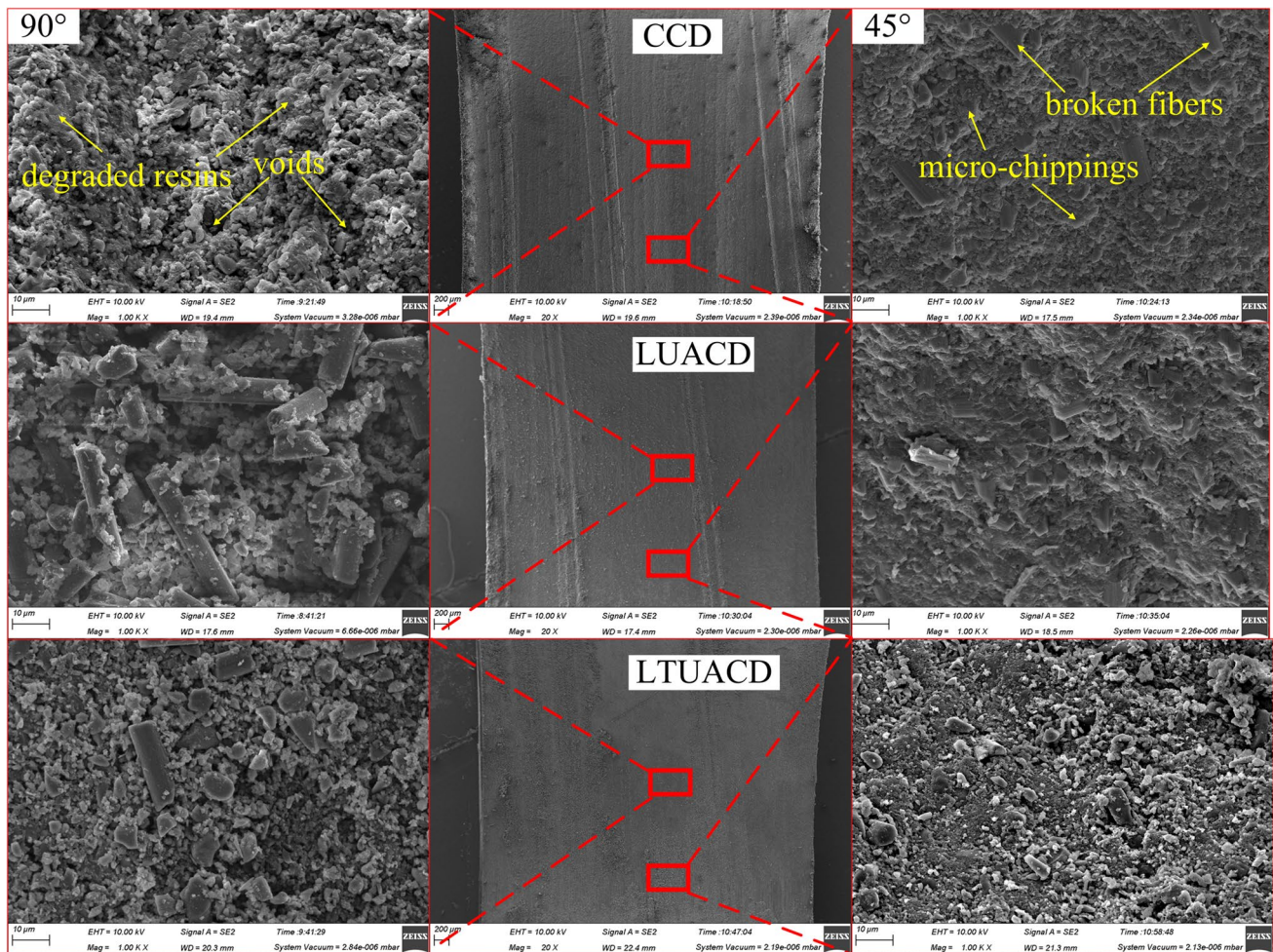


**Fig. 17** Surface morphologies of hole wall at fiber cutting angle of 45° and 90° in CCD, LUACD, and LTUACD ( $n=3000$  r/min,  $v_f=10$  mm/min,  $A=1$   $\mu$ m)

adhesion and maintains the tool cutting ability. At the same time, the static cutting process of CCD is changed and chip evacuation conditions are improved because the machining process becomes separated cutting state because of additional ultrasonic, which enhances tool sharpness and cutting ability to easily cut off fibers. This accelerates fiber fracture and obtains more flat fiber fracture surfaces (Fig. 17).

## 5 Conclusions

In this paper, the machining performance of LTUACD of CFRP is analyzed from the aspect of cutting force. And the exit delamination reduction mechanism of LTUACD of CFRP is discussed. Then, a series of experiments were conducted to verify the analysis. Main conclusions are as follows:

1. The cutting force is significantly reduced in LTUACD of CFRP compared to CCD and LUACD. Specifically, due to the effect of intermittent cutting of ultrasonic vibration, the static cutting process of CCD is changed, and the contact time of abrasive grain and material is reduced, which results in the reduction of cutting force in LTUACD and LUACD compared to CCD. Moreover, due to the addition of torsional vibration on the tool, the contact time is further reduced and tool-workpiece friction is also reduced, which further reduces the cutting force in LTUACD compared to LUACD.
2. Compared to CCD and LUACD, the exit delamination of CFRP in LTUACD is smallest. This can be attributed to the ultrasonic self-cleaning function. Due to the additional torsional vibration of tool, chips are easier to separate from tool and conduce to lesser tool chip adhesion, which keeps the sharpness of tool and enhances the tool cutting ability. This is beneficial to fiber fracture and reduces tearing shear effect of rod chip.

3. The volume of fractured fibers in LTUACD is smallest under the three processing methods (CCD, LUACD, and LTUACD). The main reason is that in circumferential direction, the contact of abrasive grain and material becomes intermittent contact with the additional torsional vibration of tool in LTUACD. Then, chip evacuation conditions are improved because of separated cutting characteristic of additional ultrasonic. Except for the shear action of abrasive grain to material, the effect of impact of vibration further accelerates fiber fracture and reduces the volume of fractured fibers. Then, this process obtains more flat fiber fracture surfaces.
4. The tool cutting ability is enhanced, fiber fracture surfaces are flatter, matrix damage is reduced, and hole surface integrity is better in LTUACD compared with CCD and LUACD because the machining process becomes separated cutting state because of additional ultrasonic; chips are difficult to stick on tool because of high-frequency vibration, and machining surface becomes smoother because of reciprocating scratches of abrasives with the addition of torsional vibration on the tool. Therefore, the machining performance of LTUACD is enhanced.

**Author contribution** ZiQiang Zhang: conceptualization, methodology, data analysis, software, writing—original draft. Feng Jiao: conceptualization; methodology; writing—review; editing—manuscript; funding acquisition; supervision. Yuanxiao Li: data collection, investigation, software. Ying Niu: material preparation, software, supervision. Jinglin Tong: experiment design, investigation, resources.

**Funding** The research is supported financially by National Natural Science Foundation of China (No. 51675164) and Fundamental Research Funds for the Universities of Henan Province (No. NSFRF200102).

## Declarations

**Ethical approval** Not applicable.

**Consent to participate** Not applicable.

**Consent for publication** Not applicable.

**Conflict of interests** The authors declare no competing interests.

## References

1. Geng D, Liu Y, Shao Z, Zhang M, Jiang X, Zhang D (2019) Delamination formation and suppression during rotary ultrasonic elliptical machining of CFRP. *Compos B Eng* 183:107698. <https://doi.org/10.1016/j.compositesb.2019.107698>
2. Li Y, Jiao F, Zhang Z, Feng Z, Niu Y (2022) Research on entrance delamination characteristics and damage suppression strategy in drilling CFRP/Ti6Al4V stacks. *J Manuf Process* 76:518–531. <https://doi.org/10.1016/j.jmapro.2022.02.018>
3. Wu CQ, Gao GL, Li HN, Luo H (2019) Effects of machining conditions on the hole wall delamination in both conventional and ultrasonic-assisted CFRP drilling. *Int J Adv Manuf Technol* 104(5–8):2301–2315. <https://doi.org/10.1007/s00170-019-04052-y>
4. Gemi L, Morkavuk S, Köklü U, Gemi D (2019) An experimental study on the effects of various drill types on drilling performance of GFRP composite pipes and damage formation. *Compos B Eng* 172:186–194. <https://doi.org/10.1016/j.compositesb.2019.05.023>
5. Tsao CC, Hocheng H (2004) Taguchi analysis of delamination associated with various drill bits in drilling of composite material. *Int J Mach Tool Manu* 44(10):1085–1090. <https://doi.org/10.1016/j.ijmactools.2004.02.019>
6. Cadorin N, Zitoun R (2015) Wear signature on hole defects as a function of cutting tool material for drilling 3D interlock composite. *Wear* 332–333:742–751. <https://doi.org/10.1016/j.wear.2015.01.019>
7. Cong WL, Pei ZJ, Treadwell C (2014) Preliminary study on rotary ultrasonic machining of CFRP/Ti stacks. *Ultrasonics* 54(6):1594–1602. <https://doi.org/10.1016/j.ultras.2014.03.012>
8. Feng Q, Cong WL, Pei ZJ, Ren CZ (2012) Rotary ultrasonic machining of carbon fiber-reinforced polymer: feasibility study. *Mach Sci Technol* 16(3):380–398. <https://doi.org/10.1080/10910344.2012.698962>
9. Zhang D, Wang H, Burks AR, Cong W (2020) Delamination in rotary ultrasonic machining of CFRP composites: finite element analysis and experimental implementation. *Int J Adv Manuf Technol* 107(9–10):3847–3858. <https://doi.org/10.1007/s00170-020-05310-0>
10. Lv D, Chen M, Yao Y, Yan C, Chen G, Zhu Y (2021) High-frequency vibration effects on the hole integrity in rotary ultrasonic drilling of carbon fiber-reinforced plastic composites. *Ultrasonics* 115:106448. <https://doi.org/10.1016/j.ultras.2021.106448>
11. Ning F, Wang H, Cong W (2019) Rotary ultrasonic machining of carbon fiber reinforced plastic composites: a study on fiber material removal mechanism through single-grain scratching. *Int J Adv Manuf Technol* 103(1–4):1095–1104. <https://doi.org/10.1007/s00170-019-03433-7>
12. Baraheni M, Amini S (2019) Comprehensive optimization of process parameters in rotary ultrasonic drilling of CFRP aimed at minimizing delamination. *Int J Lightweight Mater Manuf* 2(4):379–387. <https://doi.org/10.1016/j.ijlmm.2019.03.003>
13. Thirumalai Kumaran S, Ko TJ, Li C, Yu Z, Uthayakumar M (2016) Rotary ultrasonic machining of woven CFRP composite in a cryogenic environment. *J Alloy Compo* 698:984–993. <https://doi.org/10.1016/j.jallcom.2016.12.275>
14. Shi H, Yuan S, Li Z, Song H, Qian J (2019) Evaluation of surface roughness based on sampling array for rotary ultrasonic machining of carbon fiber reinforced polymer composites. *Measurement* 138:175–181. <https://doi.org/10.1016/j.measurement.2019.02.002>
15. Li Z, Zhang D, Qin W, Geng D (2016) Removal analyses of chip and rod in rotary ultrasonic-assisted drilling of carbon fiber-reinforced plastics using core drill. *J Reinf Plast Comp* 35(15):1173–1190. <https://doi.org/10.1177/0731684416644510>
16. Amini S, Baraheni M, Mardiha A (2018) Parametric investigation of rotary ultrasonic drilling of carbon fiber reinforced plastics. *Proc Inst Mech Eng Part E* 232(5):540–554. <https://doi.org/10.1177/0954408917727199>
17. Chen F, Bie W, Wang X, Zhao B (2022) Longitudinal-torsional coupled rotary ultrasonic machining of ZrO<sub>2</sub> ceramics: an experimental study. *Ceram Int* 48(19):28154–28162. <https://doi.org/10.1016/j.ceramint.2022.05.398>

18. Wang J, Zhang J, Feng P, Guo P, Zhang Q (2018) Feasibility study of longitudinal–torsional-coupled rotary ultrasonic machining of brittle material. *J Manuf Sci Eng* 140(5):051008. <https://doi.org/10.1115/1.4038728>
19. Geng D, Zhang D, Xu Y, He F, Liu F (2014) Comparison of drill wear mechanism between rotary ultrasonic elliptical machining and conventional drilling of CFRP. *J Reinf Plast Comp* 33(9):797–809. <https://doi.org/10.1177/0731684413518619>
20. Liu J, Zhang D, Qin L, Yan L (2011) Feasibility study of the rotary ultrasonic elliptical machining of carbon fiber reinforced plastics (CFRP). *Int J Mach Tool Manu* 53(1):141–150. <https://doi.org/10.1016/j.ijmachtools.2011.10.007>
21. Geng D, Lu Z, Yao G, Liu J, Li Z, Zhang D (2017) Cutting temperature and resulting influence on machining performance in rotary ultrasonic elliptical machining of thick CFRP. *Int J Mach Tool Manu* 123:160–170. <https://doi.org/10.1016/j.ijmachtools.2017.08.008>
22. Cong WL, Pei ZJ, Sun X, Zhang C (2013) Rotary ultrasonic machining of CFRP: a mechanistic predictive model for cutting force. *Ultrasonics* 54(2):663–675. <https://doi.org/10.1016/j.ultras.2013.09.005>
23. Chen M, Zhao Q, Dong S, Li D (2004) The critical conditions of brittle–ductile transition and the factors influencing the surface quality of brittle materials in ultra-precision grinding. *J Mater Process Tech* 168(1):75–82. <https://doi.org/10.1016/j.jmatprotec.2004.11.002>
24. Lu Y, Yuan S, Chen Y (2019) A cutting force model based on kinematic analysis in longitudinal and torsional ultrasonic vibration drilling. *Int J Adv Manuf Technol* 104(1–4):631–643. <https://doi.org/10.1007/s00170-019-03884-y>
25. Faraz A, Biermann D, Weinert K (2009) Cutting edge rounding: an innovative tool wear criterion in drilling CFRP composite laminates. *Int J Mach Tool Manu* 49(15):1185–1196. <https://doi.org/10.1016/j.ijmachtools.2009.08.002>
26. Wang J, Feng P, Zhang J, Shen H (2017) Experimental investigation on the effects of thermomechanical loading on the vibrational stability during rotary ultrasonic machining. *Mach Sci Tech* 21(2):239–256. <https://doi.org/10.1080/10910344.2017.1283962>
27. Geng D, Teng Y, Liu Y, Shao Z, Jiang X, Zhang D (2019) Experimental study on drilling load and hole quality during rotary ultrasonic helical machining of small-diameter CFRP holes. *J Mater Process Tech* 270:195–205. <https://doi.org/10.1016/j.jmatprotec.2019.03.001>
28. Krishnaraj V, Prabukarthi A, Ramanathan A, Elanghovan N, Senthil Kumar M, Zitoun R, Davim JP (2012) Optimization of machining parameters at high speed drilling of carbon fiber reinforced plastic (CFRP) laminates. *Compos B Eng* 43(4):1791–1799. <https://doi.org/10.1016/j.compositesb.2012.01.007>

**Publisher's note** Springer Nature remains neutral with regard to jurisdictional claims in published maps and institutional affiliations.

Springer Nature or its licensor (e.g. a society or other partner) holds exclusive rights to this article under a publishing agreement with the author(s) or other rightsholder(s); author self-archiving of the accepted manuscript version of this article is solely governed by the terms of such publishing agreement and applicable law.